# Implementation and Analysis of a Control Scheme for Damping of Oscillations in VSC-based HVDC Grids

Salvatore D'Arco*

*SINTEF Energy Research
7465 Trondheim Norway
salvatore.darco@sintef.no
Jon.A.Suul@sintef.no

Jon Are Suul*†

†Department of Electric Power Engineering
Norwegian University of Science and Technology
7495 Trondheim, Norway

Marta Molinas#

#Department of Engineering Cybernetics
Norwegian University of Science and Technology
7495 Trondheim, Norway
marta.molinas@ntnu.no

***Abstract* — This paper proposes a simple method for damping of oscillations in dc grids based on Voltage Source Converters (VSCs). The damping effect is achieved by a control loop for counteracting measured dc voltage oscillations by acting on the active current reference of the ac-side VSC controller. The design of the damping method is supported by participation factor analysis and parametric sensitivities of a small-signal model representing an investigated test case. This investigated system is consisting of a single HVDC converter station connected to a dc cable equivalent and an ac grid. The validity of the developed small-signal model is verified by comparison to a simulation model including nonlinear effects of the investigated converter configuration. The small-signal model is then used to analyze the stability and dynamic characteristics of the system with and without the proposed active damping and to identify a suitable tuning of the damping controller.**

***Keywords-Active damping, eigenvalue analysis, dc grids, small-signal modelling, voltage oscillations, Voltage Source Converter***

## I. INTRODUCTION

More than a century after the dominance of ac power transmission was established, the advent of versatile Voltage Source Converters (VSCs) in a wide voltage and power range has marked the re-emergence of power transmission in dc-grids as a relevant option. However, as ac transmission still has the significant advantage of electromagnetic transformers with high efficiency for adapting the voltage levels of various generation units and loads, dc grids are mainly becoming relevant in particular targeted applications [1]. Among the possible applications of dc grids, the potential for VSC-based multi-terminal High Voltage dc (HVDC) transmission systems is being envisioned as a relevant option for enabling large scale power transmission over long distances [2]. This is especially relevant for offshore transmission systems, where the capacitance of subsea ac cables effectively limits the achievable transmission distance. Thus, future plans for large-scale offshore wind farms, electrification of oil and gas installations and offshore cross-border interconnections in the North Sea region, is expected to be based on VSC HVDC connections which can be expanded into an interconnected multi-terminal dc grid [2]-[4].

Cables for both ac and dc power transmission exhibit higher distributed capacitance values compared to overhead lines. Thus, cable-based connections over long distances imply the presence of significant inductance and stray capacitance in the system, causing multiple LC resonance frequencies. It is also known that the presence of LC resonances in cable-based ac systems can cause poorly damped oscillations, over-voltages and even instability due to interactions with power electronic converters and their control systems [5]-[9]. Thus, the inductive and capacitive effects of HVDC cables can have significant impact on the system stability and response to transient events of VSC-based HVDC grids, even if they will not have any influence on the steady-state power flow and control characteristics. In systems with long dc cables, resonances can appear at a relatively low frequency, increasing the possibility for interaction with the converter control loops [10]. The possibility for oscillations interacting with converter control systems can also be further increased by the presence of inductive fault current limiters installed as part of the protection scheme for HVDC grids.

In general, the damping of LC oscillations depends on the presence of dissipative elements in the circuit. Arguably the easiest measure to reduce the presence of oscillations is the intentional introduction of resistive elements, which is commonly applied for damping LC or LCL input filers of converters [11], [12]. However, for such passive damping, the attenuation of the oscillations is accompanied by higher losses, which is not compatible with the objective of maximizing efficiency in high power systems. Especially in HVDC configurations, minimization of losses is of critical importance, since they will significantly influence the system lifetime cost.

In the last decades, alternative approaches for damping of oscillations and suppression of harmonics caused by LC resonances without introducing physical resistances in the circuit have been proposed. This has been possible due to the controllability of power electronic converters, and has led to the introduction of concepts as Active Damping and Virtual Resistances, where the effect of dissipative elements is fictitiously mimicked by the converter control [7], [9], [13]-[16]. With such control methods, the behavior in terms of damping effect is similar to the effect of a real resistance but

The work of SINTEF Energy Research in this paper was supported by the project "Protection and Fault Handling in Offshore HVDC Grids," (ProOfGrids), financed by the Norwegian Research Council's RENERGI program and the industry partners (EDF, GE, National Grid, Siemens, Statkraft, Statnett, Statoil and NVE) http://www.sintef.no/Projectweb/ProOfGrids/

978-1-4799-2060-0/14/$31.00 ©2014 IEEE

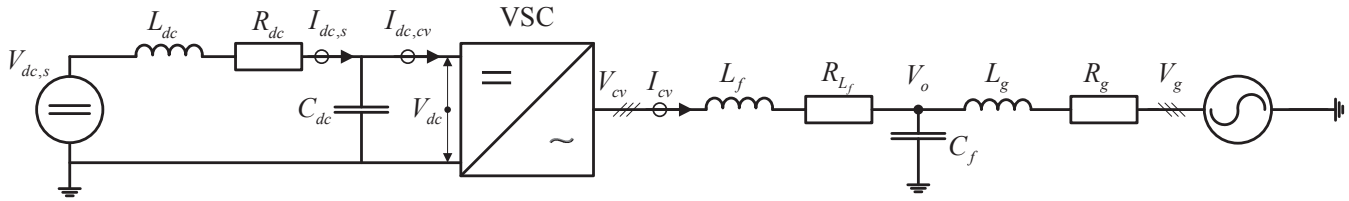


**Fig. 1. Overview of electrical system for a HVDC converter terminal**

without introducing any physical losses. This has been particularly relevant for ac grid connected converters with LC or LCL filters, but has also been considered for avoiding filter instabilities of DC-DC converters in low power applications [17], [18]. However, methods for active damping are not commonly applied for reduction of oscillations in high power, high voltage, dc systems.

The similarities in the behavior of an LC filter circuit and high voltage ac or dc cables suggest the possibility to introduce the principle of active damping also for avoiding oscillations caused by the cable characteristics. This has already been considered for attenuating oscillations in the ac cables of collection grids for wind farms as discussed in [7] and [9]. In this paper, it is proposed to apply similar approaches for damping of oscillations in the dc cables of VSC-based HVDC transmission systems. A mathematical model of an HVDC terminal with its basic controller functionality is derived as a basis for analyzing the proposed approach for dc-side active damping. The analytical derivations include the development of a small-signal model of the system for stability assessment based on linear techniques. The operation of the proposed active damping method and the validity of the linearized model are demonstrated by numerical simulations of a sample case. The linearized model is then used for verifying and analyzing the suitability of the proposed active damping controller and its impact on the dynamic performance of the investigated system.

## II. Mathematical Model for a VSC Converter with AC and DC Active Damping

In the following sub-sections, a mathematical model of a VSC converter in a typical HVDC configuration as shown in Fig. 1 will be presented. The model will include simplified representations of the ac-side and dc-side electrical systems, conventional ac-side control loops and the proposed strategy for damping of dc voltage oscillations.

### A. Modelling conventions

In the system configuration from Fig. 1, upper case symbols represent physical values of the electrical circuit, while the control system implementation and the modelling of the system will be based on per unit quantities denoted by lower case letters. The base values for the per unit system are defined from the apparent power rating of the converter and the peak value of the rated phase voltage [19].

The modelling, analysis and control of the electrical system on the ac-side will be presented in a Synchronous Reference Frame (SRF) aligned with the voltage vector $\boldsymbol{v}_o$ at the filter capacitor $C_f$. The transformation of three-phase voltage and current measurements from the stationary reference frame into the SRF is based on the amplitude-invariant Park

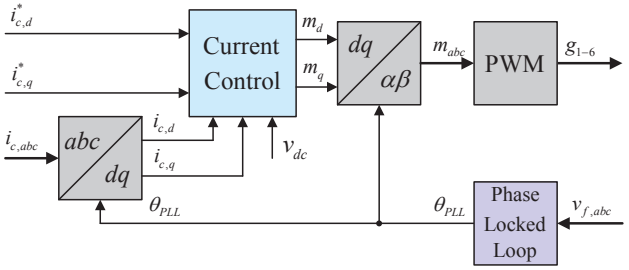


**Fig. 2. Overview of basic control system structure**

transformation, with the d-axis aligned with the voltage vector $\boldsymbol{v}_o$ and the q-axis leading the d-axis by 90° [19]. Thus, the magnitude of current and voltage vectors at rated conditions is 1.0 pu. Whenever possible, SRF equations will be presented in complex space vector notation according to (1).

$$\mathbf{x} = x_d + j \cdot x_q \tag{1}$$

### B. Electrical System Model and Conventional Control

The electrical system to be modelled was indicated in Fig. 1, and an overview of the fundamental elements of the control structure for the VSC is shown in Fig. 2.

#### 1) Electrical System on the ac-side

Assuming an LC filter as the grid interface of the VSC converter and a Thévenin equivalent representation of the grid, the state-space equations of the ac-side electrical circuit model can be established as given by (2) [20], [21].

$$\begin{aligned}
\frac{d\mathbf{i}_{cv}}{dt} &= \frac{\omega_b}{l_f}\mathbf{v}_{cv} - \frac{\omega_b}{l_f}\mathbf{v}_o - \left(\frac{r_{l_f}\omega_b}{l_f} + j\cdot\omega_g\omega_b\right)\mathbf{i}_{cv} \\
\frac{d\mathbf{v}_o}{dt} &= \frac{\omega_b}{c_f}\mathbf{i}_{cv} - \frac{\omega_b}{c_f}\mathbf{i}_o - j\cdot\omega_g\omega_b\cdot\mathbf{v}_o \\
\frac{d\mathbf{i}_o}{dt} &= \frac{\omega_b}{l_g}\mathbf{v}_o - \frac{\omega_b}{l_g}\mathbf{v}_g - \left(\frac{r_g\omega_b}{l_g} + j\cdot\omega_g\omega_b\right)\mathbf{i}_o
\end{aligned} \tag{2}$$

The voltages, currents and circuit elements of these equations are indicated in Fig. 1, while $\omega_g$, is the per unit grid frequency. The base angular grid frequency is defined by $\omega_b$.

#### 2) Power Balance and Electrical System on the DC-Side

An ideal lossless average model is assumed for the converter, imposing a power balance constraint between the ac- and the dc-side of the converter as given by:

$$v_{cv,d}\cdot i_{cv,d} + v_{cv,q}\cdot i_{cv,q} = v_{dc}\cdot i_{dc,cv} \tag{3}$$

The dc-side electrical systems is modelled as an equivalent voltage source $v_{dc,s}$ connected to the converter through a dc cable represented by a single pi-equivalent section. This pi-equivalent section is modelled by the cable resistance $R_{dc}$, the corresponding inductance $L_{dc}$ and the stray capacitance of the cable. However, the capacitance of the pi-equivalent is not

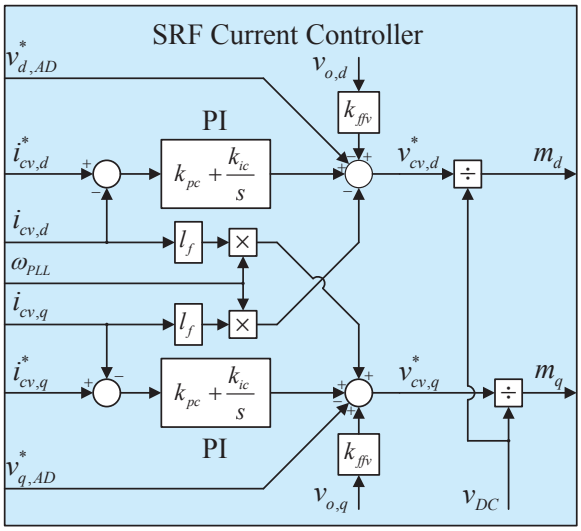


**Fig. 3. Current Controller**

included in parallel with the dc source, since the voltage at this point is fixed to the source voltage. The equivalent capacitance on the other side of the cable is directly in parallel with the dc-link capacitor of the VSC and is therefore incorporated in the capacitance given by $C_{dc}$. It can be noted that this representation is very simplified and can approximate only the lowest frequency resonant peak of the cable [10]. However, this choice represents also a worst case scenario with respect to the damping of LC oscillations, since the oscillatory effects that in a real cable would be spread on several frequencies are condensed in a single resonant frequency. It can also be noted that the same model could be used to represent an inductive fault current limiter connected to the dc-link capacitor of the VSC. The dc-side of the converter can then be modelled in a state-space representation by two dynamic equations according to:

$$\frac{dv_{dc}}{dt} = \frac{\omega_b}{c_{dc}} i_{dc,s} - \frac{\omega_b}{c_{dc}} i_{dc} \tag{4}$$

$$\frac{di_{dc,s}}{dt} = \frac{\omega_b}{l_{dc}} v_{dc,s} - \frac{\omega_b}{l_{dc}} v_{dc} - \frac{\omega_b \cdot r_{dc}}{l_{dc}} i_{dc,s} \tag{5}$$

*3) Current Controllers and ac Active Damping*

The inner loop current controllers of the VSM control structure are assumed to be conventional SRF PI controllers with decoupling terms, and are shown in Fig. 3 [20], [21]. Thus, the output voltage reference from the PI controller is defined by $\boldsymbol{v}^*_{cv}$ according to (6), where the current reference tracked by the controller is given by $\boldsymbol{i}^*_{cv}$. The proportional and integral gains of the PI controller are defined by $k_{pc}$ and $k_{ic}$, and the state $\boldsymbol{\gamma}$ is defined to represent the integrators of the PI controllers according to (7).

$$\mathbf{v}^*_{cv} = k_{pc}\left(\mathbf{i}^*_{cv} - \mathbf{i}_{cv}\right) + k_{ic} \cdot \boldsymbol{\gamma} + j \cdot l_1 \cdot \omega_{PLL} \cdot \mathbf{i}_{cv} + k_{ffv} \cdot \mathbf{v}_o - \mathbf{v}^*_{AD} \tag{6}$$

$$\frac{d\boldsymbol{\gamma}}{dt} = \mathbf{i}^*_{cv} - \mathbf{i}_{cv} \tag{7}$$

In (6), a gain factor $k_{ffv}$, which can be set to 0 or 1, is used to disable or enable the voltage feed-forward in the output of the current controllers. The decoupling terms of the controllers are based on the per unit grid frequency $\omega_{PLL}$ estimated by the

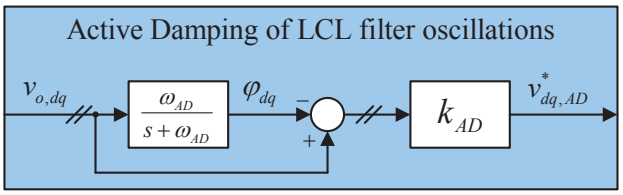


**Fig. 4. AC-side Active Damping**

Phase Locked Loop used for grid synchronization, as will be explained in the following subsection.

The voltage reference for the converter also includes an active damping term designed for suppressing LC oscillations in the filter [14], [15]. Although several concepts for active damping of such filter oscillations have been developed, the simple approach applied in this case is based on adding a component in the converter output voltage which is in counter-phase with the detected oscillations, in order to produce a cancellation effect. Thus, the oscillations are first isolated by high-pass filtering and the resulting signal is then multiplied by a gain and added to the output reference as shown in Fig. 4. This structure implements active damping in a synchronous reference frame and assumes the availability of the dq-components of the measured voltage at the filter capacitors which in ideal steady-state conditions will appear as constant. The high-pass filter function is implemented by subtracting from the measured voltage signals a low-pass filtered version of the same voltages. Indeed, the damping voltage reference $\boldsymbol{v}^*_{AD}$ in (6) is based on the difference between the measured filter voltage $\boldsymbol{v}_o$ and the low-pass filtered value of the same voltage, scaled by the gain $k_{AD}$, as given by (8) The corresponding internal states $\boldsymbol{\varphi}$ of the d- and q- axis low-pass filters are defined by (9), where $\omega_{AD}$ is the cut-off frequency of the applied low-pass filter.

$$\mathbf{v}^*_{AD} = k_{AD}\left(\mathbf{v}_o - \boldsymbol{\varphi}\right) \tag{8}$$

$$\frac{d\boldsymbol{\varphi}}{dt} = \omega_{AD} \cdot \mathbf{v}_o - \omega_{AD} \cdot \boldsymbol{\varphi} \tag{9}$$

The active damping gain and the cutoff frequency of the low-pass filter represent two tuning parameters that can be selected in order to adapt the dynamic response of the active damping. Indeed, a lower cutoff frequency and a higher gain produce a stronger attenuation of oscillations and a more damped response. However, low cut-off frequency of the low-pass filters and high values of $k_{AD}$ will also cause the active damping to resist natural changes of operating conditions for the converter, and will therefore result in a slower dynamic response of the system to changes in external set-points.

For the actual implementation of the VSC control system, the voltage reference $\boldsymbol{v}^*_{cv}$ resulting from the current controller and the active damping is divided by the measured dc-link voltage to result in the modulation index $m$ as shown to the right of Fig. 3. However, the instantaneous average value of the per unit converter output voltage is given by the product of the modulation index and the actual dc-voltage. Thus, neglecting the switching operation of the converter and any delay due to the PWM implementation, the output converter voltage will be approximately equal to the voltage reference as given by (10).

$$\mathbf{m} = \frac{\mathbf{v}^*_{cv}}{v_{dc}}, \qquad \mathbf{v}_{cv} = \mathbf{m} \cdot v_{dc} \quad \rightarrow \mathbf{v}_{cv} \approx \mathbf{v}^*_{cv} \tag{10}$$

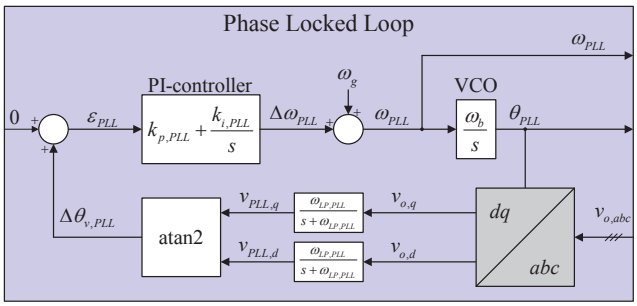


**Fig. 5. Phase Locked Loop**

*4) Phase Locked Loop*

The Phase Locked Loop (PLL) used to track the actual grid frequency is shown in Fig. 5 and is based on [22], [23]. This PLL is using first order low-pass filters on the estimated d- and q-axis voltages and an inverse tangent function to estimate the actual phase angle error of the PLL. This phase angle error is the input to a PI controller tracking the frequency of the measured voltage, which is integrated to obtain the estimate of the actual phase angle.

The states of the low-pass filters of the PLL, resulting in the filtered voltage $\boldsymbol{v}_{PLL}$, is given by (11) where the cut-off frequency of the applied low-pass filters is given by $\omega_{LP,PLL}$.

$$\frac{d\mathbf{v}_{PLL}}{dt} = -\omega_{LP,PLL} \cdot \mathbf{v}_{PLL} + \omega_{LP,PLL} \cdot \mathbf{v}_o \tag{11}$$

The integrator state $\varepsilon_{PLL}$ of the PI controller is defined by (12), and the speed deviation $\delta\omega_{PLL}$ of the PLL with respect to the grid frequency is defined by (13) for SRF small-signal modelling. The corresponding phase angle difference between the grid voltage $\boldsymbol{v}_g$ and the orientation of the PLL is represented by $\delta\theta_{PLL}$ as defined by (14).

$$\frac{d\varepsilon_{PLL}}{dt} = \arctan\left(\frac{v_{PLL,q}}{v_{PLL,d}}\right) \tag{12}$$

$$\delta\omega_{PLL} = k_{p,PLL} \cdot \arctan\left(\frac{v_{PLL,q}}{v_{PLL,d}}\right) + k_{i,PLL} \cdot \varepsilon_{PLL} \tag{13}$$

$$\frac{d\delta\theta_{PLL}}{dt} = \delta\omega_{PLL} \cdot \omega_b \tag{14}$$

This implies that the grid voltage represented by its amplitude $\hat{v}_g$ can be transformed into the PLL reference frame used to model the system as given by:

$$\mathbf{v}_g = \hat{v}_g e^{-j\delta\theta_{PLL}} \tag{15}$$

The grid frequency deviation $\delta\omega_{PLL}$ and the phase angle displacement $\delta\theta_{PLL}$ from (13) and (14) are necessary for modelling of the PLL in the SRF. However, for implementation of the control system, the actual instantaneous voltage vector phase angle estimated by the PLL, which will be monotonously increasing in the range between 0 and 2π, is needed for transformation between the stationary and synchronously rotating reference frames. This phase angle will be given by the integral of the actual per unit frequency $\omega_{PLL}$ as defined by (16). Thus, the state-space representation of the instantaneous phase angle $\theta_{PLL}$ of the PLL oriented SRF, as detected by the PLL and used in the dq-transformations indicated in Fig. 2, is given by (17).

$$\omega_{PLL} = \delta\omega_{PLL} + \omega_g \tag{16}$$

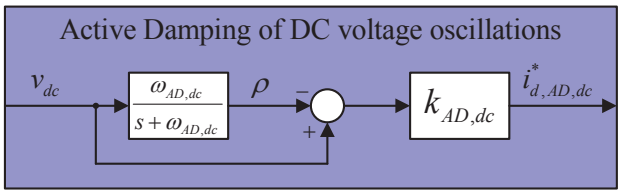


**Fig. 6. DC-side Active Damping**

$$\frac{d\theta_{PLL}}{dt} = \omega_{PLL} \cdot \omega_b \tag{17}$$

## C. Proposed Active Damping of DC Voltage Oscillations

The active damping approach proposed for attenuating oscillations in the dc-side of the converter is from a functional point of view identical to the ac active damping described in the previous section and is also similar to the approach commonly used for active filters [24]. Thus, the same approach of isolating the oscillating component of the voltage by high-pass filtering is applied, as shown by the block diagram in Fig. 6. The detected oscillatory component is in this case multiplied by a gain to produce a current reference that can be used to stabilize the measured voltage of the dc-link capacitor of the converter. Since the damping of oscillations in the dc-link capacitor requires that the power flow through the converter is modified, the current reference resulting from the proposed active dc damping is labelled as $i^*_{AD,dc}$ and added directly to the d-axis current reference for the ac side current controllers as given by (18). In this equation, $i^{r*}_{cv,d}$ is the external d-axis current reference for the converter, which might be directly specified or calculated from an external active power command, while $\rho$ is defined as the state of the low-pass filter used for implementing the active damping, as defined by (19).

$$i^*_{cv,d} = i^{r*}_{cv,d} + i^*_{AD,dc} = i^{r*}_{cv,d} + k_{AD,dc}\left(v_{dc} - \rho\right) \tag{18}$$

$$\frac{d\rho}{dt} = -\omega_{AD,dc} \cdot \rho + \omega_{AD,dc} \cdot v_{dc} \tag{19}$$

It can be clearly seen from Fig. 6 that the active damping will be effectively disabled if the gain $k_{AD,dc}$ is set to zero. However, if the low-pass filter crossover frequency is set to zero, assuming an initial state of 0, it can be seen that the block diagram of Fig. 6 will result in a current that is directly proportional to the measured dc voltage. This would imply that the active damping gain $k_{AD,dc}$ would appear as a virtual conductance added in shunt with the dc capacitor voltage. Thus, the normal operation of the proposed active damping method can be considered to have the effect of a transient damping resistance that is inserted in parallel with the dc capacitor and only reacts to oscillations or fast changes in the dc voltage. The suitability of this approach and its influence on the dynamic characteristics of the system will be further investigated by analysis of a linearized small-signal model in the following sections.

## D. Small-Signal Modelling

By combining the equations presented in the previous section, the system can be modelled in a state-space representation through a nonlinear model of 17th order. The nonlinearity of the model prevents the direct application of classical linear analysis techniques. Thus, a small-signal representation is derived for the system in the form of (20).

$$\Delta\dot{\mathbf{x}} = \mathbf{A}\cdot\Delta\mathbf{x} + \mathbf{B}\cdot\Delta\mathbf{u} \tag{20}$$

The prefix Δ denotes small-signal deviations around the steady-state operating point, while **x** is the vector of the state variables and **u** is the input vector. The state and input vectors used for the modelling are given by (21).

$$\mathbf{x} = \begin{bmatrix} v_{o,d} & v_{o,q} & i_{l,d} & i_{l,q} & \gamma_d & \gamma_q & i_{o,d} & i_{o,q} & \varphi_d & \varphi_q \\ & & & v_{PLL,d} & v_{PLL,q} & \varepsilon_{PLL} & \delta\theta_{PLL} & v_{dc} & i_{dc} & \rho \end{bmatrix}^T \tag{21}$$

$$\mathbf{u} = \begin{bmatrix} i_{l,q}^* & i_{l,d}^{r*} & v_{dc,s} & \hat{v}_g & \omega_g \end{bmatrix}^T$$

The A- and B-matrices of the resulting small-signal state-space model are given by (22) and (23), where the elements $k_{7,14}$, $k_{8,14}$, $k_{15,3}$, $k_{15,4}$ and $k_{15,15}$ of the A-matrix are specified by (24)-(28).

$$\mathbf{B} = \begin{bmatrix} 0 & 0 & 0 & 0 & 0 \\ 0 & 0 & 0 & 0 & -\omega_b v_{o,d,0} \\ 0 & \frac{\omega_b k_{pc}}{l_f} & 0 & 0 & 0 \\ \frac{\omega_b k_{pc}}{l_f} & 0 & 0 & 0 & 0 \\ 0 & 1 & 0 & 0 & 0 \\ 1 & 0 & 0 & 0 & 0 \\ 0 & 0 & 0 & -\frac{\omega_b \cos(\delta\theta_{PLL,0})}{l_g} & \omega_b i_{o,q,0} \\ 0 & 0 & 0 & -\frac{\omega_b \sin(\delta\theta_{PLL,0})}{l_g} & -\omega_b i_{o,d,0} \\ 0 & 0 & 0 & 0 & 0 \\ 0 & 0 & 0 & 0 & 0 \\ 0 & 0 & 0 & 0 & 0 \\ 0 & 0 & 0 & 0 & 0 \\ 0 & 0 & 0 & 0 & 0 \\ 0 & 0 & 0 & 0 & 0 \\ -\frac{\omega_b k_{pc} i_{l,q,0}^*}{c_{dc} v_{dc,0}} & -\frac{\omega_b k_{pc} i_{l,d,0}^*}{c_{dc} v_{dc,0}} & 0 & 0 & 0 \\ 0 & 0 & \frac{\omega_b}{l_{dc}} & 0 & 0 \\ 0 & 0 & 0 & 0 & 0 \end{bmatrix} \tag{23}$$

$$k_{7,14} = \frac{\omega_b \hat{v}_{g,0} \sin(\delta\theta_{PLL,0})}{l_g} \tag{24}$$

$$k_{8,14} = \frac{\omega_b \hat{v}_{g,0} \cos(\delta\theta_{PLL,0})}{l_g} \tag{25}$$

TABLE I PARAMETERS OF INVESTIGATED SYSTEM CONFIGURATION

| Parameter | Value | Parameter | Value |
|---|---|---|---|
| Rated voltage $V_{S,LL,RMS}$ | 220 kV | Filter inductance $l_f$ | 0.08 pu |
| Rated power $S_b$ | 1200 MVA | Filter resistance $r_{lf}$ | 0.003 pu |
| Rated angular frequency $\omega_b$ | 2π*50 Hz | Filter capacitance $c_f$ | 0.074 pu |
| Initial current reference $i^{r*}_{cv,d}$ | −0.5 pu | Grid inductance $l_g$ | 0.20 pu |
| Equivalent dc capacitor, $c_{dc}$ | 4.2 pu | Grid resistance $r_g$ | 0.01 pu |
| DC cable inductance, $l_{dc}$ | 0.5 pu | Grid voltage $\hat{v}_g$ | 1.0 pu |
| DC cable resistance, $r_{dc}$ | 0.007 pu | DC source voltage $v_{dc,s}$ | 1.0 pu |

$$k_{15,3} = \omega_b \frac{k_{pc} i_{l,d,0}^* - k_{ffv} v_{o.d.0} - k_{ic} \gamma_{d,0}}{c_{dc} v_{dc,0}} \tag{26}$$

$$k_{15,4} = \omega_b \frac{k_{pc} i_{l,q,0}^* - k_{ic} \gamma_{q,0}}{c_{dc} v_{dc,0}} \tag{27}$$

$$k_{15,15} = \omega_b \frac{-k_{pc} k_{AD,dc} i_{l,d,0}^* v_{dc,0} + k_{ffv} i_{l,d,0}^* v_{o,d,0} + k_{ic} i_{l,d,0}^* \gamma_{d,0} + k_{ic} i_{l,q,0}^* \gamma_{q,0}}{c_{dc} v_{dc,0}^2} \tag{28}$$

## III. SYSTEM ANALYSIS

As a point of reference, the electrical system from Fig. 1 is simulated in Simulink/SimPowerSystems by using an average model of a VSC converter, controlled by the control loops presented in the previous section. The parameters listed in Table I will be used as a starting point for the simulations. Regarding these parameters, it should be remembered that the dc parameters are scaled into per unit by using the same base frequency as for the ac side, resulting in apparently high values for per unit inductance and capacitance. However, these parameters are corresponding to a dc cable of about 70 km.

### *A. Model Verification and Active Damping Performance*

In the following, the operation of the proposed active damping and the validity of the developed small-signal model will be investigated. The results from simulations with the full nonlinear simulation model are therefore compared with results obtained from the linearized state-space model without and with the active damping enabled. The validated small-signal

$$\mathbf{A} = \begin{bmatrix} 0 & \omega_b\omega_{g,0} & \frac{\omega_b}{c_f} & 0 & 0 & 0 & -\frac{\omega_b}{c_f} & 0 & 0 & 0 & 0 & 0 & 0 & 0 & 0 & 0 & 0 \\ -\omega_b\omega_{g,0} & 0 & 0 & \frac{\omega_b}{c_f} & 0 & 0 & 0 & -\frac{\omega_b}{c_f} & 0 & 0 & 0 & 0 & 0 & 0 & 0 & 0 & 0 \\ \omega_b\frac{k_{ffv}-1-k_{AD}}{l_f} & 0 & -\omega_b\frac{k_{pc}+r_f}{l_f} & 0 & \omega_b\frac{k_{ic}}{l_f} & 0 & 0 & 0 & \omega_b\frac{k_{AD}}{l_f} & 0 & 0 & -\omega_b\frac{k_{p,PLL}i_{l,q,0}^*}{v_{o,d,0}} & -\omega_b k_{i,PLL} i_{l,q,0}^* & 0 & \omega_b\frac{k_{pc}k_{AD,dc}}{l_f} & 0 & -\omega_b\frac{k_{pc}k_{AD,dc}}{l_f} \\ 0 & \omega_b\frac{k_{ffv}-1-k_{AD}}{l_f} & 0 & -\omega_b\frac{k_{pc}+r_f}{l_f} & 0 & \omega_b\frac{k_{ic}}{l_f} & 0 & 0 & 0 & \omega_b\frac{k_{AD}}{l_f} & 0 & \omega_b\frac{k_{p,PLL}i_{l,d,0}^*}{v_{o,d,0}} & \omega_b k_{i,PLL} i_{l,d,0}^* & 0 & 0 & 0 & 0 \\ 0 & 0 & -1 & 0 & 0 & 0 & 0 & 0 & 0 & 0 & 0 & 0 & 0 & 0 & k_{AD,dc} & 0 & -k_{AD,dc} \\ 0 & 0 & 0 & -1 & 0 & 0 & 0 & 0 & 0 & 0 & 0 & 0 & 0 & 0 & 0 & 0 & 0 \\ \frac{\omega_b}{l_g} & 0 & 0 & 0 & 0 & 0 & -\frac{\omega_b r_g}{l_g} & \omega_b\omega_{g,0} & 0 & 0 & 0 & 0 & 0 & k_{7,14} & 0 & 0 & 0 \\ 0 & \frac{\omega_b}{l_g} & 0 & 0 & 0 & 0 & -\omega_b\omega_{g,0} & -\frac{\omega_b r_g}{l_g} & 0 & 0 & 0 & 0 & 0 & k_{8,14} & 0 & 0 & 0 \\ \omega_{AD} & 0 & 0 & 0 & 0 & 0 & 0 & 0 & -\omega_{AD} & 0 & 0 & 0 & 0 & 0 & 0 & 0 & 0 \\ 0 & \omega_{AD} & 0 & 0 & 0 & 0 & 0 & 0 & 0 & -\omega_{AD} & 0 & 0 & 0 & 0 & 0 & 0 & 0 \\ \omega_{LP,PLL} & 0 & 0 & 0 & 0 & 0 & 0 & 0 & 0 & 0 & -\omega_{LP,PLL} & 0 & 0 & 0 & 0 & 0 & 0 \\ 0 & \omega_{LP,PLL} & 0 & 0 & 0 & 0 & 0 & 0 & 0 & 0 & 0 & -\omega_{LP,PLL} & 0 & 0 & 0 & 0 & 0 \\ 0 & 0 & 0 & 0 & 0 & 0 & 0 & 0 & 0 & 0 & 0 & \frac{1}{v_{o,d,0}} & 0 & 0 & 0 & 0 & 0 \\ 0 & 0 & 0 & 0 & 0 & 0 & 0 & 0 & 0 & 0 & 0 & \frac{\omega_b k_{p,PLL}}{v_{o,d,0}} & \omega_b k_{i,PLL} & 0 & 0 & 0 & 0 \\ \omega_b\frac{(k_{AD}-k_{ffv})i_{l,d,0}^*}{c_{dc}v_{dc,0}} & \omega_b\frac{(k_{AD}-k_{ffv})i_{l,q,0}^*}{c_{dc}v_{dc,0}} & k_{15,3} & k_{15,4} & -\omega_b\frac{k_{ic}i_{l,d,0}^*}{c_{dc}v_{dc,0}} & -\omega_b\frac{k_{ic}i_{l,q,0}^*}{c_{dc}v_{dc,0}} & 0 & 0 & -\omega_b\frac{k_{AD}i_{l,d,0}^*}{c_{dc}v_{dc,0}} & -\omega_b\frac{k_{AD}i_{l,q,0}^*}{c_{dc}v_{dc,0}} & 0 & 0 & 0 & 0 & k_{15,15} & \frac{\omega_b}{c_{dc}} & -\omega_b\frac{k_{pc}k_{AD,dc}i_{l,d,0}^*}{c_{dc}v_{dc,0}} \\ 0 & 0 & 0 & 0 & 0 & 0 & 0 & 0 & 0 & 0 & 0 & 0 & 0 & 0 & -\frac{\omega_b}{l_{dc}} & -\frac{\omega_b r_{dc}}{l_{dc}} & 0 \\ 0 & 0 & 0 & 0 & 0 & 0 & 0 & 0 & 0 & 0 & 0 & 0 & 0 & 0 & \omega_{AD,dc} & 0 & -\omega_{AD,dc} \end{bmatrix} \tag{22}$$

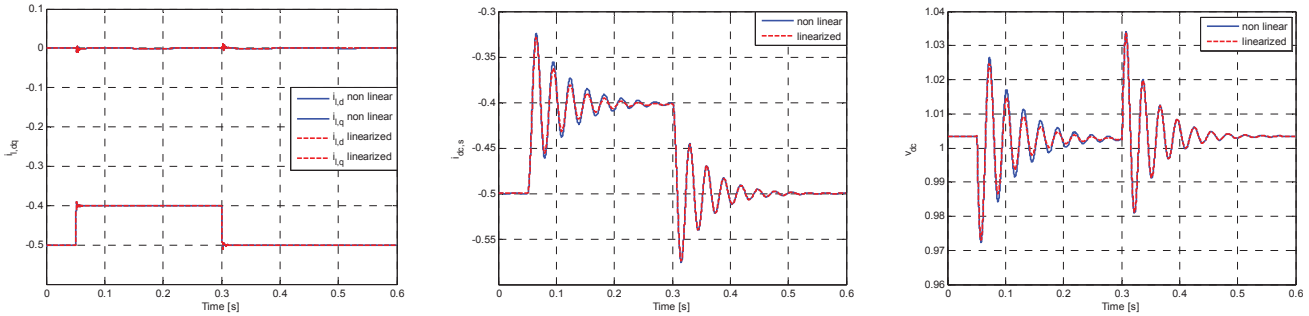


a) d- and q- axis currents b) current in the dc-line c) dc voltage

**Fig. 7. System response for 0.1 pu step in active current reference $i_d$ on the ac-side and without active damping of dc voltage oscillations.**

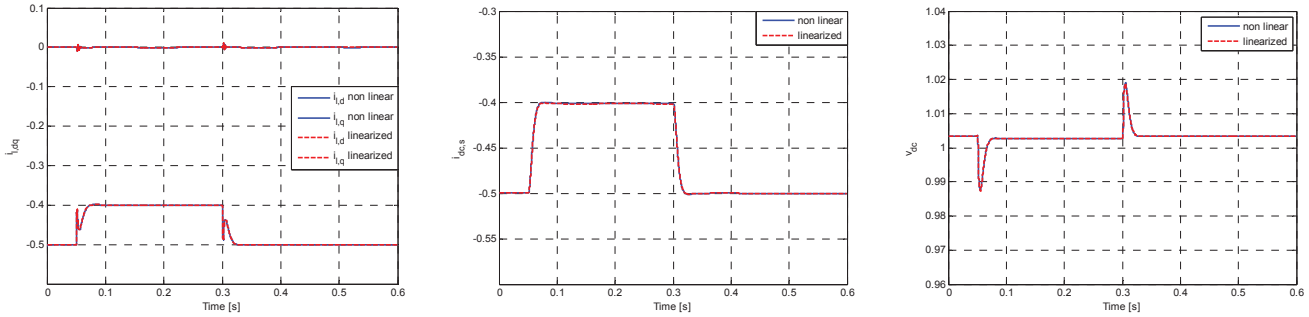


a) d- and q- axis currents b) current in the dc-line c) dc volage

**Fig. 8. System response for 0.1 pu step in active current reference $i_d$ on the ac-side and active damping of dc voltage oscillations activated**

model is then used to further analyze the characteristics of the investigated system.

*1) Operation without Active Damping*

In Fig. 7 the response of the system without the active damping is shown when the d-axis current reference for the converter is stepped from −0.5 pu to −0.4 pu, corresponding to a 0.1 pu reduction of power transferred from the ac side to the dc-side, and then back again to the initial operating point. The response of the d- and q-axis currents on the ac-side to this change of current reference is shown in Fig. 7 a), where it is clear that the response is fast and well damped. The current in the dc cable is shown in Fig. 7 b), while the corresponding dc voltage is shown in Fig. 7c), and it can be noticed that both curves show a poorly damped oscillation. The figures also include a comparison between the nonlinear and the linearized model, where it can be seen that there is no noticeable deviation between the ac signals of the two models. On the dc-side, is can be noticed that the linearized small-signal model is accurately capturing the oscillation frequency of the dc voltage and current, while there is a small deviation in the amplitude and damping of the oscillations of the two models when the set-point for the control of the converter is moved away from the linearization point. This is due to the nonlinearity of the power balance from (3). However, when the current reference is stepped back to its initial value, it can be seen that there is an almost perfect match between the nonlinear and the linearized models. Thus, the linearized small-signal model can be used to accurately evaluate the stability and dynamic performance of the system around the linearization point.

*2) Operation with Active damping*

Results from simulating the same sequence of changing the current reference as in Fig. 7 when the proposed active damping of dc voltage oscillations is activated are shown in Fig. 8. In this simulation, the filter crossover frequency is 5 rad/s and the gain is 4.0 pu, and it is clearly seen from the presented plots that the dc damping is able to effectively cancel the oscillations from Fig. 7. It can also be seen from Fig. 8 a) how this damping is achieved by transiently modifying the d-axis current of the converter. This results in a smooth and well damped response of the current in the dc cable as shown in Fig. 8 b), and the dc voltage shows only a small and well damped overshot in response to the change of operating conditions as shown in Fig. 8 c). From all these curves, it can be seen that the results from the linearized models are again accurately representing the nonlinear system model. The only deviation between the two models is an expected, but almost unnoticeable, difference between the simulated dc voltages and currents when the system is brought to another operating point than used for the linearization.

## *B. System Analysis Based on Small-Signal Linearized Model*

From the linearized small-signal state-space model, system eigenvalues can easily be calculated for evaluating the stability and dynamic characteristics of the system. This also allows for applying techniques for linear system analysis, like calculation of participation factors and parametric sensitivities, to evaluate the characteristics of the various oscillation modes that can be identified in the system [19]. Thus, the appropriateness and characteristics of the proposed method for active damping of dc oscillations can be analyzed with such techniques. An example of this is demonstrated by calculating the participation factor of the oscillatory mode associated with the dc-side oscillations from Fig. 7. The result is shown in Fig. 9, where the upper plot is showing some of the eigenvalues in the system, calculated for the case without the active damping

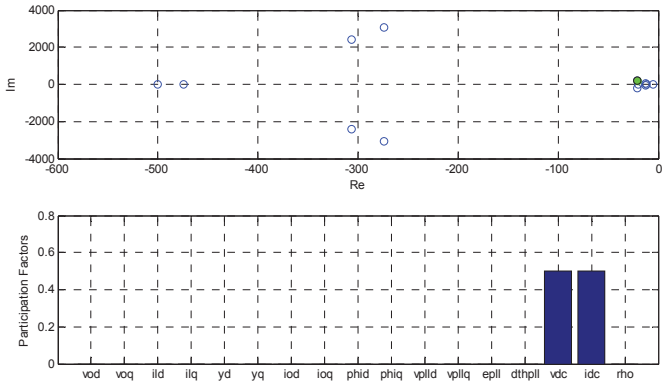


**Fig. 9. Participation factor of dc-oscillatory poles without active damping**

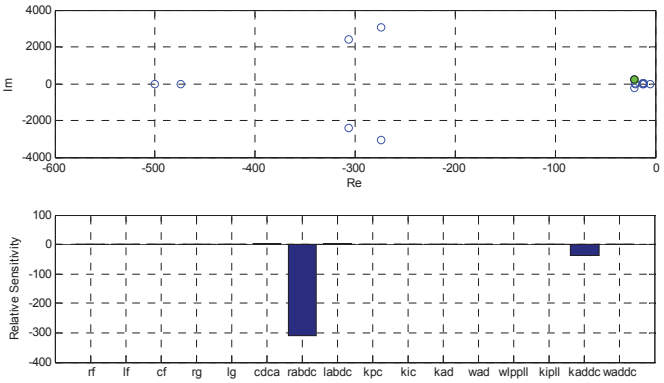


**Fig. 10. Parametric sensitivity of dc-oscillatory pole along the real axis without active damping**

enabled, with a green marker used to identify the eigenvalue associated with the dc-side oscillations. The participation factors of this eigenvalue, representing the participation of the various states in this particular oscillation mode, are shown in the lower part of Fig. 9, identifying that the two only states equally influencing these oscillations are the dc voltage and the current in the dc cable. Thus, any method for damping such oscillations should act on one of these states. Since the voltage of the dc-link capacitor is easy to measure, and is usually already available as an internal variable in the VSC control system, a damping method based on the dc voltage appears as the most appropriate option.

The parametric sensitivity of the various eigenvalues can also be easily calculated from the linearized state-space model of the system [19], [25]. Thus, the relative parametric sensitivity of the pole pair associated with the dc-oscillations is plotted in Fig. 10. As for the presented participation factor, the parametric sensitivity is calculated with the proposed active damping disabled by setting the gain $k_{AD,dc}$ to zero. However, as the active damping is included in the state-space model, the parametric sensitivity of the oscillatory eigenvalue with respect to the active damping parameters is still calculated. From the bar diagram shown in the lower part of Fig. 10, it is clearly seen that the two only parameters with strong influence on the dc oscillations in this operating condition are the resistance in the dc cable and the gain of the active damping. This verifies that the active damping is an effective approach for attenuating the oscillations. It can also be noted that even if the location of the eigenvalue representing the dc-side oscillatory behavior is much more sensitive to the cable resistance than the gain of the active damping, there will be no physical constraints on the active damping like there are for the cable resistance that directly represents losses in the system.

To further investigate the effect of the proposed active damping method on the dc-side oscillations, the root locus of all the system eigenvalues for a parametric sweep of the active damping gain $k_{AD,dc}$ is plotted in Fig. 11. For this plot, the crossover frequency of the low-pass filter used in the active damping is set to 5 rad/s corresponding to a time constant of 200 ms, while the gain is swept from 0 to 100. A color gradient indicates the direction of the parametric sweep, where blue shades of the marked eigenvalues correspond to a lower value of the gain and red shades corresponds to the highest gains. It can be noticed that the gain affects several poles and has a major impact on the system dynamics. However, the general trend of the oscillatory poles is a reduction of the imaginary component together with a shift towards the left. This corresponds to a faster damping of the oscillations. In particular, the poles associated with the dc-oscillations can be recognized from Fig. 9 and Fig. 10 as the pole-pair close to the origin, and it can be clearly seen how these poles are moved towards the left when the active damping gain is increasing from zero. However if the gain is increased too much, the pair of complex conjugate poles representing the dc oscillations are transformed into two real poles, where one is moving back towards the right, resulting in a slower response of the system. This can also be confirmed by the corresponding set of step-responses of the system obtained from the small-signal model as shown in Fig. 12, where it is seen that the dynamic response of the dc voltage becomes quite slow when the active damping gain is increased more than necessary to attenuate the oscillations. Thus an intermediate gain of the active damping, usually in the range between 1.0 and 5.0 is found to be appropriate. However, from the linearized state-space model, any range of tuning parameters and their influence on the system stability can be easily investigated. On basis of this model it is also possible to develop iterative tuning procedures for optimizing the system response as proposed in [25].

## IV. CONCLUSION

This paper has presented a possible approach for attenuation of oscillations in VSC-based HVDC grids with significant LC resonances due to long cables or the presence of inductive fault current limiters. A simple implementation for active damping of the corresponding dc voltage oscillations has been proposed, and its performance has been verified by time-domain simulations of a case study based on a typical VSC HVDC configuration. As a tool for analysis of these oscillations, a linearized small-signal state-space model of the investigated system has been developed. This model has been used to analyze the dynamic characteristics of the system and to verify the design and tuning of the proposed active damping method and provides the foundation for using simple and powerful linear analysis for exploring and assessing the stability of the system.. The analysis of participation factors and parametric sensitivities of the eigenvalues associated with dc voltage oscillation also verifies the suitability of the proposed active damping approach.

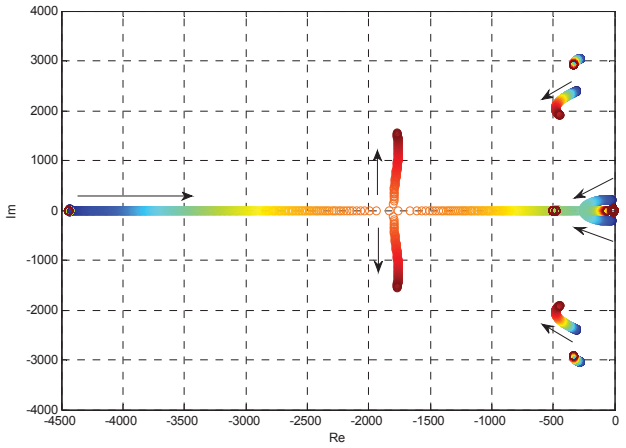


**Fig. 11. Root locus of system poles when the active damping gain $k_{AD,dc}$ is swept from 0 to 100**

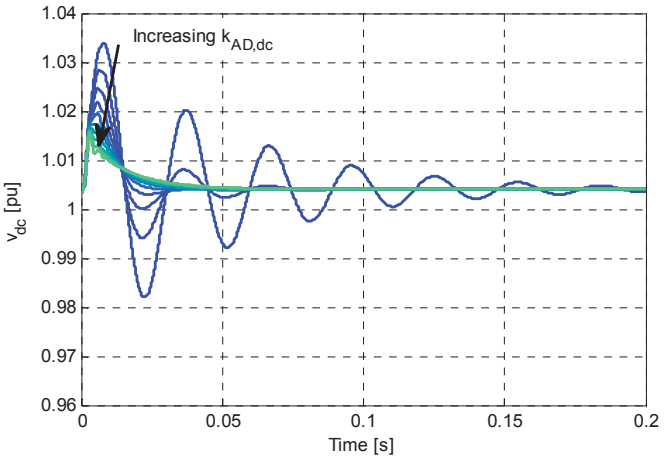


**Fig. 12. Response of dc-link voltage to a small step in ac-side active current reference $i_d$ with increasing values of $k_{AD,dc}$**

## REFERENCES


[1] M. Saeedifard, M. Graovac, R. F. Dias, R. Iravani, "DC Power Systems: Challenges and Opportunities," in *Proceedings of the IEEE PES General Meeting 2010*, Minneapolis, Minnesota, USA, 25-29 July 2010, 7 pp.

[2] S. Cole, T. K. Vrana, O. B. Fosso, J.-B. Curtis, A.-M. Denis, C.-C. Liu, "A European Supergrid: Present State and Future Challenges," in *Proceedings of the 17th Power Systems Computational Conference*, PSCC 2011, Stockholm, Sweden, 22-26 August 2011, 8 pp.

[3] The North Seas Countries' Offshore Grid Initiative, NSCOGI, information available from http://www.benelux.int/nscogi/

[4] T. K. Vrana, "*System Design and Balancing of the North Sea Super Grid*," PhD Thesis, Norwegian University of Science and Technology, 2013

[5] B. Gustavsen, "Study of Transformer Resonant Overvoltages Caused by Cable-Transformer High-Frequency Interaction," in *IEEE Transactions on Power Delivery*, Vol. 25, No. 2, April 2010, pp. 770-779

[6] J. H. R. Enslin, R. J. M. Heskes, "Harmonic Interaction Between a Large Number of Distributed Power Inverters and the Distribution Network," in *IEEE Transactions on Power Electronics*, Vol. 19, No. 6, November 2004, pp. 1586-1593

[7] M. Céspedes, J. Sun, "Modeling and Mitigation of Harmonic Resonance Between Wind Turbines and the Grid," in *Proceedings of the IEEE Energy Conversion Congress and Exposition*, ECCE 2011, Phoenix, Arizona, USA, 17-22 September 2011, pp. 2109-2116

[8] H. Liu, J. Sun, "Impedance-Based Stability Analysis of VSC-Based HVDC Systems," in *Proceedings of the 2013 IEEE 14th Workshop on Control and Modeling for Power Electronics*, COMPEL 2013, Salt Lake City, Utah, USA, 23-26 June 2013,8 pp.

[9] S. Jiang, S. Zhang, X. Lu, B. Ge, F. Z. Peng, "Resonance Issues and Active Damping in HVAC Grid-Connected Offshore Wind Farm," in *Proceedings of the 2013 IEEE Energy Conversion Congress and Exposition*, ECCE 2013, Denver, Colorado, USA, 10-19 September 2013, pp 210-215

[10] W. Wang, M. Barnes, O. Marjanovic, "Droop Control Modelling and Analysis of Multi-terminal VSC-HVDC for Offshore Wind Farms," in *Proceedings of the 10th IET International Conference on AC and DC Power Transmission*, ACDC 2012, Birmingham, UK, 4-5. December, 2012, 6 pp.

[11] T. C. Y. Wang, Z. Ye, G. Sinha, X. Yuan, "Output Filter Design for a Grid-interconnected Three-Phase Inverter," in *Proceedings of the 2003 IEEE 34th Annual Power Electornics Specialists Conference*," Acapulco, New Mexico, USA, 15-19 June 2003, pp. 779-784

[12] A. A .Rockhill, M. Liserre, R. Teodorescu, P. Rodríguez, "Grid-Filter Design for a Multimegawatt Medium-Voltage Voltage-Source Inverter," in *IEEE Transactions on Industrial Electronics*, Vol. 58, No.4, April 2011, pp. 1205-1217

[13] V. Blasko, V. Kaura, "A Novel Control to Actively Damp Resonance in Input LC Filter of a Three-Phase Voltage Source Converter," in *IEEE Transactions on Industry Applications*, Vol. 33, No. 2, March/April 1997, pp. 542-550

[14] O. Mo, M. Hernes, K, Ljøkelsøy, "Active Damping of Oscillations in LC-filter for Line Connected, Current Controlled, PWM Voltage Source Converters," in *Proc. of the 10th European Conference on Power Electronics and Applications*, EPE 2003, Toulouse, France, 2-4. September 2003, 10 pp.

[15] M. Malinowski, M. P. Kazmierkowski, S. Bernet, "New Simple Active Damping of Resonance in Three-Phase PWM Converter with LCL Filter," in *Proceedings of the 2005 IEEE International Conference on Industrial Technology*, ICIT 2005, Hong Kong, 14-17 December 2005, pp. 861-865

[16] J. Dannehl, F. W. Fuchs, S. Hansen, P. B. Thøgersen, "Investigation of Active Damping Approaches for PI-Based Current Control of Grid-Connected Pulse Widht Modulated Converters With LCL Filters," in *IEEE Transactions on Industry Applications*, Vol. 46, No. 4, July/August 2010, pp. 1509-1517

[17] A. Jusoh, "*Active Damping of DC Power Networks*," PhD Thesis, The University of Birmingham, Birmingham, UK, 2003

[18] A. M. Rahimi, A. Emadi, "Active Damping in DC/DC Power Electronic Converters: A Novel Method to Overcome the Problems of Constant Power Loads," in *IEEE Transactions on Industrial Electronics*, Vol. 56, No. 5, May 2009, pp. 1428-1439

[19] P. Kundur, "*Power System Stability and Control*," McGraw-Hill, New York, 1994

[20] V. Blasko, V. Kaura, "A New Mathematical Model and Control of a Three-Phase AC-DC Voltage Source Converter," in *IEEE Transactions on Power Electronics*, Vol. 12, No. 1, January 1997, pp. 116-123

[21] N. Kroutnikova, C. A. Hernandez-Aramburo, T. C. Green, "State-space model of grid-connected inverters under current control mode," in *IET Electric Power Applications*, Vol 1, No. 3, May 2007, pp. 329-338

[22] V. Kaura, V. Blasko, "Operation of a Phase Locked Loop System Under Distorted Utility Conditions," in *IEEE Transactions on Industry Applications*, Vol. 33, No. 1, January/February 1997, pp. 58-63

[23] H. Kolstad, "*Control of an Adjustable Speed Hydro utilizing Field Programmable Devices*," Ph.D. Thesis, Norwegian University of Science and Technology, 2002

[24] H. Akagi, E. H. Watanabe, M. Aredes, "*Instantaneous Power Theory and Applications to Power Conditioning*," IEEE Press / John Wiley & Sons, Hoboken, New Jersey, USA, 2007

[25] S. D'Arco; J. A. Suul; O. B. Fosso, "Control System Tuning and Stability Analysis of Virtual Synchronous Machines," in *Proceedings of the 2013 IEEE Energy Conversion Congress and Exposition*, ECCE 2013, Denver, Colorado, USA, 15-19 September 2013, pp. 2664-2671